Available online at www.eccomasproceedia.org
Eccomas Proceedia COMPDYN (2017) 1667-1684

ECCOMAS
Proceedia

COMPDYN 2017
6th ECCOMAS Thematic Conference on
Computational Methods in Structural Dynamics and Earthquake Engineering
M. Papadrakakis, M. Fragiadakis (eds.)
Rhodes Island, Greece, 15–17 June 2017

COMPLETE ANALYTICAL THERMOMECHANICAL MODEL OF DOUBLE FRICTION PENDULUM DEVICES

Vincenzo Bianco[1], Giorgio Monti[1] and Nicola P. Belfiore[2]

[1] Department of Structural Engineering and Geotechnics
via Antonio Gramsci n°53 00197 - Rome
{vincenzo.bianco, giorgio.monti}@uniroma1.it

[2] Department of Mechanical and Aerospace Engineering
via Eudossiana n°18, 00184 - Rome
nicolapio.belfiore@dima.uniroma1.it

Keywords: Base Isolation, Friction Pendulum Devices, Dynamical Behavior, Non-Linear Modelling.

Abstract. *Friction Pendulum Devices (FPDs) are strongly attracting the attention of both Academic and Technical Communities of Engineers concerned with the development of strategies for the protection of structures against earthquakes. Several versions of such devices can be found on the market, ranging from the Single, to the Double and up to the so-called Triple Friction Pendulum. Those devices are characterized by an increasing number of kinematic pairs and corresponding sliding plates. Even though their effectiveness has extensively been proven by means of numerous experimental campaigns carried out worldwide, it seems that many aspects concerning their mechanical behavior still need to be clarified. These aspects concern, among others: 1) the sequence of sliding on the several concave surfaces, 2) the influence of temperature on the frictional properties of the coupling surfaces, 3) the possibility of alternation of mechanical sticking and slipping phases, 4) the possibility of impact-induced rupture of some components, and so on. Those aspects are less clear the larger the number of concave surfaces the device is composed of. With the aim to contribute to a better understating of the mechanical behavior of the multiple friction pendulum devices, a new mechanical interpretation of their behavior was formulated and the relevant model was developed. Such model is based on a rigorous, though simplified, mechanical approach. Starting from the analysis of a double pendulum device, which comprises two stainless steel concave plates facing each other and a convex-faced pad coated with polytetrafluoroethylene (PTFE), the mechanical model envisages the decomposition of each time-instant of the dynamic time-history in two phases. For each phase the device is modelled by an open kinematic chain of rigid bodies differently constrained between each other. Moreover, the model is based on the fulfillment of 1) geometric compatibility, 2) kinematic compatibility, 3) dynamical equilibrium and 4) thermo-mechanical coupling.*

Peer-review under responsibility of the organizing committee of COMPDYN 2017.
doi: 10.7712/120117.5521.18268

1 INTRODUCTION

Friction pendulum devices, since their early introduction [1] have earned increasing attention as a valid alternative to elastomeric bearings, for the seismic protection of both buildings, low to medium-rise, and bridges. The resulting relevant scientific output ranges from early studies on the friction properties of the kinematic pair, mainly composed so far of PolyTetraFluoroEthylene (PTFE) and stainless steel (*e.g.* [2-3]), to the proposal of many prototypes and their mechanical modelling (*e.g.* [4-8]), and up to the study of the overall behavior of an isolated structure (*e.g.* [9]). Such devices are based on the principle of obtaining the decoupling between the movement of the structure and the underlying ground by means of the relative sliding between coupled spherical surfaces, one of which in plain polished stainless steel and the other coated by a particular material chosen to ensure a suitable value of the friction coefficient. The spherical shape of the two surfaces forming a kinematic pair is supposedly necessary in order to provide the device with self-re-centering capability. The simplest of such devices envisages the presence of one only of these spherical kinematic pairs even though proposals of prototypes with multiple sliding surfaces can be found both in literature and on the market (*e.g.* [8]). The larger the number of coupling surfaces the device is composed, the more difficult the mechanical behavior under earthquake attack prediction appears to be. In the present work, attention is focused on the so-called Double Friction Pendulum (DFP) device (Fig. 1).

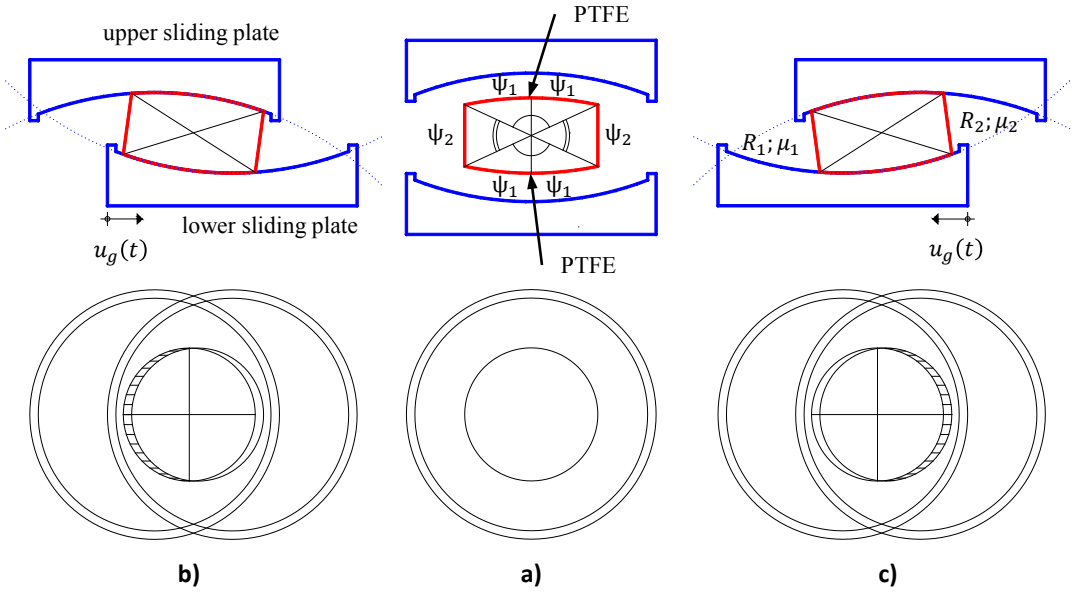

Figure 1: Friction pendulum bearing with two spherical kinematic pairs (Double Friction Pendulum DFP): a) several components, deformed shape assumed for either b) rightward or c) leftward movement of the lower plate.

One of the aspects that has been largely investigated is the mathematical model of the horizontal force-displacement hysteretic curve, which needs to be implemented in the Finite Element Models (FEM) of isolated structures in order to carry out the dynamic analyses. Most of the proposals that can be found in the literature seem to face the problem from a planar and too simplistic point of view. In fact, they seem to be based on horizontal equilibrium only, thus completely neglecting both rotational and vertical equilibrium. Moreover, they assume that sliding takes place on a strict sequence of kinematic pairs the given device is be composed of. However, few attention has been paid so far to the geometrical compatibility fulfilled by the several components during an earthquake induced deformation time-history.

Moreover, such complex tribological systems are known to be susceptible to 1) the stick-slip and 2) the sprag-slip phenomena (*e.g.* [10]). Where: the former consists of the likely alternation of time intervals of sliding to time intervals of absence of sliding, with consequent re-coupling of the ground shaking and superstructure movement, while the latter consists of vibrations that may activate in the direction orthogonal to the sliding one.

In this scenario, many questions arise about the actual functioning of these devices. Do the kinematic pairs actually undergo sliding? Do they always re-center? Otherwise, under which specific boundary conditions, either kinematic (displacements, velocities and accelerations history) or tribological (friction) do they re-center? Similarly to what happens with a rolling wheel, must friction have an optimum value, for sliding to take place? In this view, would a limit value of asymptotically null friction allow those devices to work, or would it rather inhibit the triggering of the functioning of the devices? Is it only friction, at each phase of the device deformation, that dictates the triggering, rather than the inhibition, of sliding along the various concave surfaces? How does rotational equilibrium affect this aspect? Does the over-structure actually horizontally translate only, without any rotation, even during an earthquake lacking the vertical component? Otherwise, under which specific conditions does not the over-structure undergo any rotation? Would it be necessary to outfit the isolation system with supplemental devices meant to suppress any possibility of rotation? Does the building actually move upward, as a response of the horizontal two-dimensional earthquake? Or rather, may it move downwards as function of the soil deformability, in order to accommodate vertical deformations? Does a complex soil-structure interaction take place during an earthquake?

It is evident that the topic is complex and needs to be faced from a multidisciplinary standpoint, involving also both mechanical and tribological engineering expertize (*e.g.* [11,12]).

With the aim to contribute to a better understanding of the mechanical behavior of the multiple FPs, thus attempting to answer the questions above, this work presents a new approach to model the thermo-mechanical behavior of such devices. It assumes, as a first approximation, that all the components the device is made of can be modelled as rigid bodies, thus neglecting, at least for the time being, any deformation. This modelling approach aims at fulfilling: 1) geometrical compatibility, 2) kinematic compatibility, 3) dynamic equilibrium, both translational and rotational, and 4) thermo-mechanical coupling.

2 MECHANICAL MODEL

2.1 Geometric compatibility

It is preferable to start by analyzing the behavior of a double friction pendulum, composed of the internal pad and only two external plates, in a radial plane, which means in case of unidirectional imposed horizontal displacement (Fig. 2). Such device also represents the internal assemblage, called articulated slider [6,7], of a Triple Friction Pendulum (TFP) so that the utility to deal with it first, is twofold. The first and most important constraint is represented by the fact that the two outermost horizontal surfaces, lower and higher, can undergo a rigid body motion remaining horizontal, which means that they can only translate remaining parallel to themselves. This is due to the fact that, at the extrados of the so-called *isolation plane*, which basically refers to the layer containing the low-stiffness devices, the various isolators are connected by a rigid diaphragm (*e.g.* [13,14]) that compels them to move synchronously while, at the intrados, to the presence of the ground. In order for that condition to be fulfilled, and to prevent any penetration of matter, it is necessary that the two external surfaces (S_1 and S_2) undergo sliding simultaneously (Figs. 1 and 2). For this reason, the friction coefficient should be the same along each of those two sliding pairs, *i.e.* $\mu_1 = \mu_2 = \mu$.

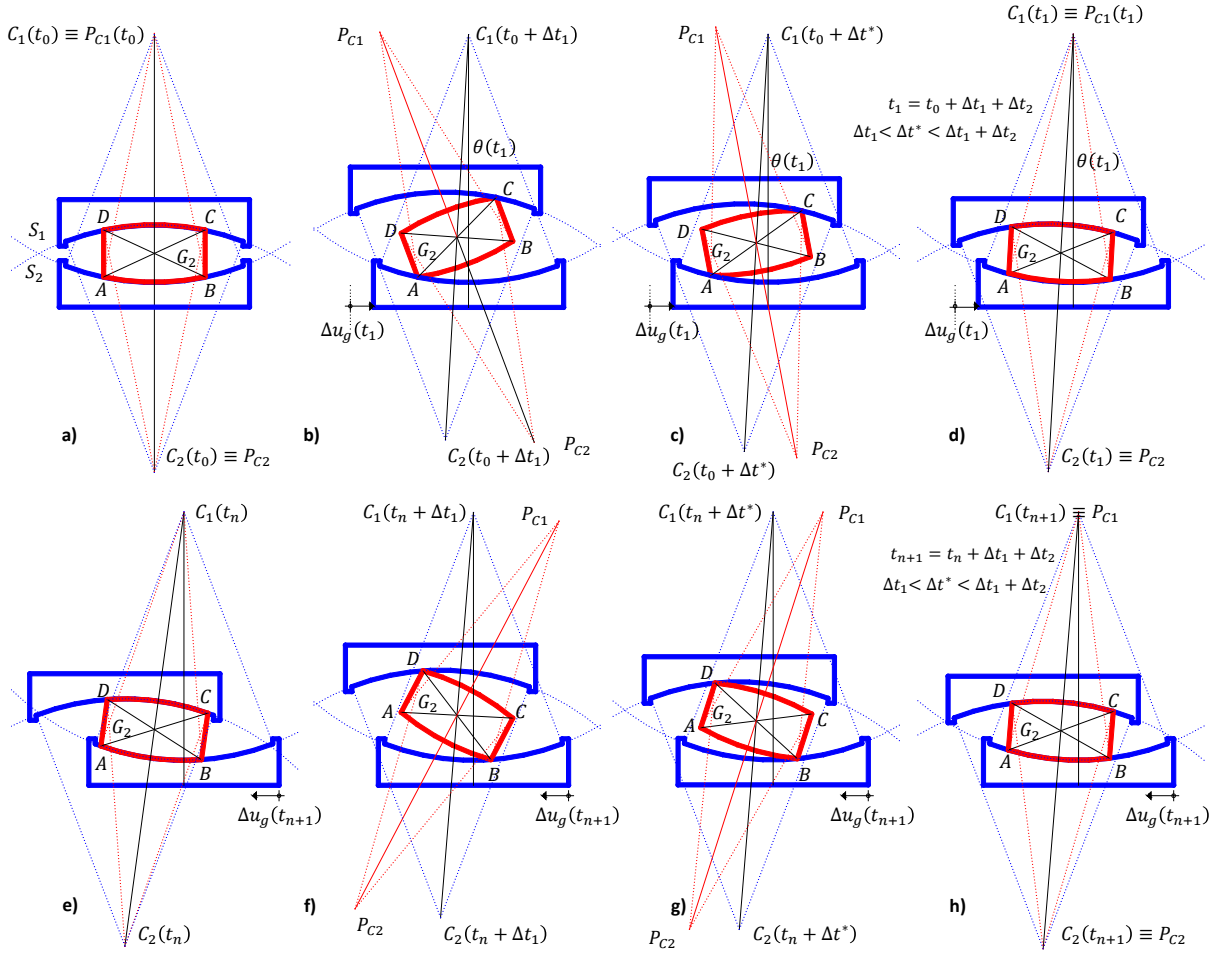

Figure 2. Assumed geometrical compatibility for the case of a DFP device subjected to a horizontal ground displacement contained in a radial plane: a-d) rightward ground movement starting from a rest position, and e-h) leftward movement starting from a maximum deformation.

At a generic time step t_n, the internal deformation undergone, as function of the imposed displacement $\Delta u_g(t_n)$, by the several components constituting the device, may be decomposed into two subsequent phases (Fig.2), even though the overall movement is contextual. When starting from the equilibrium undeformed condition (Fig. 2a-d), in the first phase, which means during the first part Δt_1 of the time increment Δt, the pad, due to the imposed displacement $\Delta u_g(t_1)$, rigidly rotates around one of the lowermost corners (A) and such rotation also yields a certain vertical displacement of the upper plate. During the second phase Δt_2 of the current time increment Δt, the pad undergoes a rigid rotation around its centroid (G_2) with this latter simultaneously rigidly translating along the straight line connecting the centers of the two spherical surfaces $\overline{C_1C_2}$. This latter direction, resulting from the end of the previous sub-interval Δt_1, is inclined, with respect to the vertical direction, of an angle $\theta(t_1)$ that is the geometrical variable (polar angle) accounting for the final configuration assumed by the entire device (Fig. 2d). The same two-step deformation can be recognized if, at a generic time step t_n, the ground imposes a reversed displacement, and starting from a generic deformed configuration (Fig. 2e-h). The only difference, in case of reversal, is that initial rigid rotation (Δt_1) involves the other diagonal of the pad (*i.e.* $\overline{DB}$ instead of $\overline{AC}$). During the second phase, sliding occurs along the corners of the involved diagonal of the pad, and friction is mobilized thereinTwo-phases mechanical model

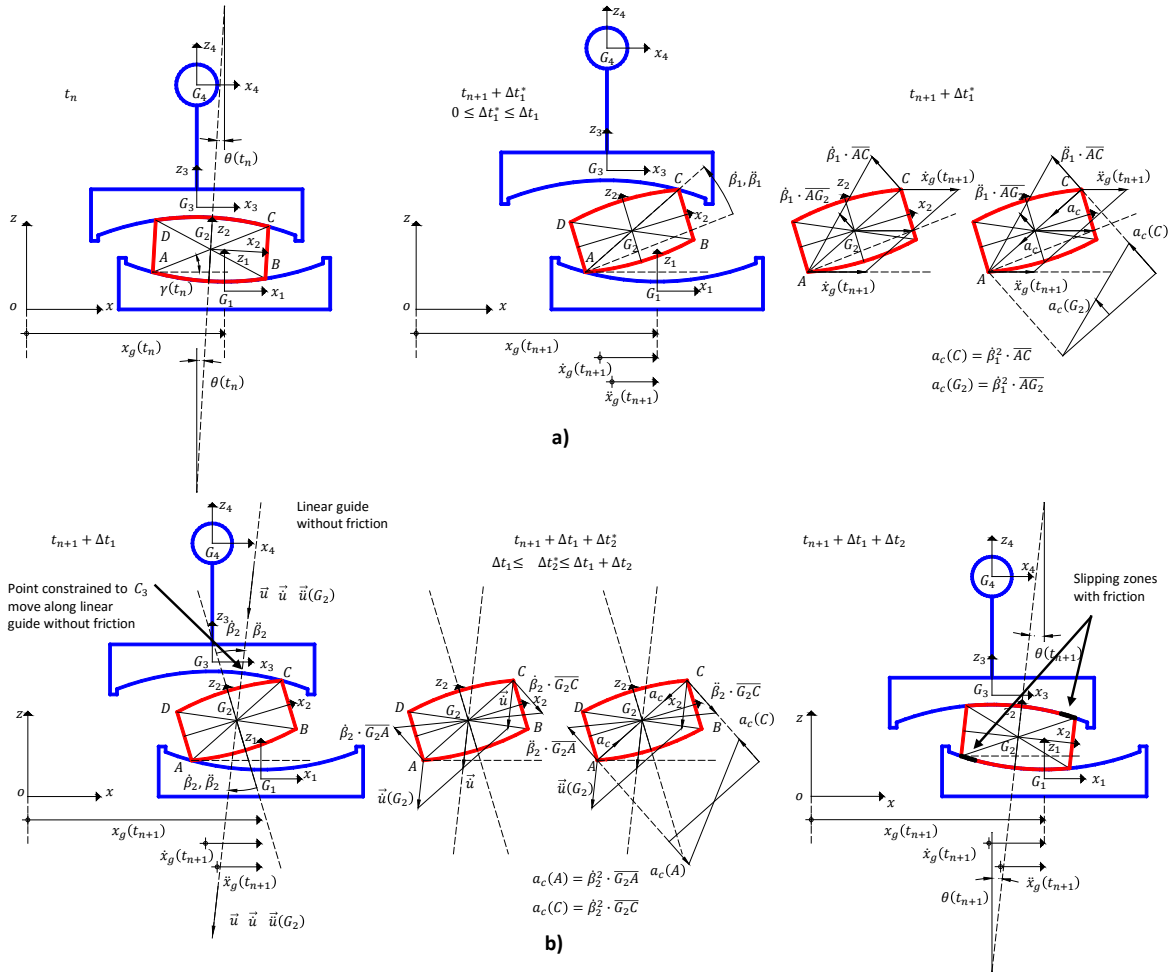

Figure 3: Mechanical models, constituted of Articulated System of Rigid Bodies (ASRB), to simulate the two-phases behavior of the DFP at a given time step: a) first phase ASRB and b) second phase ASRB.

The analysis of the geometric compatibility of the friction pendulum devices described in the previous section suggests, in a consequential manner, the way in which it is possible to model the mechanical behavior of such devices also in the three dimensional space [15,16]. For the reasons already explained in the previous section, in the present work attention is focused on the dynamical behavior of a DFP subjected to a ground shaking, leaving the study of complete TFP to further future developments. Moreover, the study is herein limited to the case of unidirectional seismic attack. The dynamical behavior of a DFP at the instant t_n can therefore be limited to what happens in the generic plane π, singled out by 1) current position of the pad $(\theta(t_n), \varphi(t_n)$ that are the polar and azimuthal angle, respectively), and 2) direction, in the global reference system $oxyz$, of the current horizontal displacement $\Delta u_g(t_{n+1})$ imposed by the ground shaking. We exclude any vertical earthquake, for the time being. Both phases at the current time step can be modelled by an *articulated system of rigid bodies*, different for each phase (Fig. 3). Even though the rigid bodies are expected to actually undergo some deformations, for the time being they are herein assumed to behave as perfectly rigid bodies. These latter form an open kinematic chain for both phases of motion (*e.g.* [17]).

During the first phase (Δt_1), the lower plate (Rigid Body 1) is assumed to move horizontally along a prismatic guide, without friction, and the motion is the one imposed by the earthquake and characterized by given displacement $x_g(t_{n+1})$, velocity $\dot{x}_g(t_{n+1})$, and acceleration

$\ddot{x}_g(t_{n+1})$. The pad (Rigid Body 2) is kinematically constrained to both lower and upper plate (RB 1,3) by two revolute joints in which the constraint force tangent to the concave surface is blocked to the maximum allowable Coulomb friction force. The upper sliding plate (RB 3) carries the weight of the over-structure that is herein assumed as a mass, rigidly connected to the plate by a massless rigid rod, and concentrated in Rigid Body 4 (RB4). Substantially, RB3 and RB4 are herein assumed to form a single rigid body assemblage. Due to the motion imposed on rigid body 1, rigid body 2 undergoes a rigid rotation β_1 around one of its corners (point A in Fig. 3a) characterized by angular velocity and acceleration $\dot{\beta}_1$, $\ddot{\beta}_1$. As a consequence of that (unknown) rotation, the assemblage of rigid bodies 3 and 4 undergoes a rigid planar translation, along axes x and z of the inertial global reference system $oxyz$, maintaining contact with the pad in the pin-joint in point C of the pad. Note that the position assumed by the plates at the end of this first phase already singles out the final updated value of the inclination of the pad with respect to both the sliding plates $\theta(t_{n+1})$.

The second phase is modelled by the same assemblage of rigid bodies above, kinematically constrained between one another in a different way (Fig. 3b). Rigid body 1 is blocked in its final position corresponding to the current time step t_{n+1}. Rigid body 2 undergoes a rigid roto-translation with its centroid G_2 translating along the straight line connecting the two centers of curvature of the two plates, along a linear prismatic guide without friction and contemporarily counter-rotates around its centroid with angular velocity and acceleration $\dot{\beta}_2$, $\ddot{\beta}_2$. Along the vertices of the diagonal involved ($\overline{AC}$ in Fig. 3), the pad is now constrained to the two plates (rigid bodies 1 and 3) by two circular guides with Coulomb friction so that, during this phase, slipping takes place with consequent yielding of heat (Fig. 3b). The kinematic quantities $\vec{\ddot{u}}(G_2)$ and $\ddot{\beta}_2$, which are the linear and angular accelerations characterizing the pad rigid roto-translation, are unknown since they depend on the dynamical characteristics of the system. On the contrary, the values of displacement $\vec{u}(G_2)$ and rotation β_2 that are necessary to restore the geometrical compatibility by closing both kinematic couples can be known by geometric relatioships at the end of the first step. The closure of both kinematic couples implies that the pad axis $\overline{P_{C1}P_{C2}}$ superimposes to the straight $\overline{C_1C_2}$ line connecting the concave plates centers (compare previous sections). The assemblage of rigid bodies 3 and 4 translate with point C_3 moving (Fig. 3b), without friction, along the straight line connecting the concave surfaces' centers $\overline{C_1C_2}(t_n + \Delta t_1)$.

2.2 Assumptions

We have made, for the time being, the following assumptions: 1) each component substantially behaves as a rigid body, 2) the stick-slip phenomenon takes place at each time step, with consequent stepwise loss and restoration of geometric compatibility, which means opening and closure of the kinematic pairs, 3) the likelihood of impact between the sub-components during the restoration of the geometric compatibility is neglected.

2.3 Kinematic Compatibility

A kinematic analysis, meant to study motion without considering the forces that produce it, is necessary. During the first phase, the velocity of point C, in which a revolute joint is placed, is given by (*e.g.* [11,12]):

$$\overrightarrow{v_C} = \overrightarrow{v_A} - \dot{\beta}_1 \cdot \vec{e}_2 \times \overrightarrow{AC} = \dot{x}_g \cdot \vec{e}_1 - \dot{\beta}_1 \cdot \vec{e}_2 \times \overrightarrow{AC} \quad (1)$$

where $\vec{e}_2$ is the unit vector of axis y of the Inertial system $oxyz$ whose positive direction is towards the paper. While the acceleration is given by:

$$\overrightarrow{a_C} = \overrightarrow{a_A} + \overrightarrow{a_c}(C) - \ddot{\beta}_1 \cdot \vec{e}_2 \times \overrightarrow{AC} = \ddot{x}_g \cdot \vec{e}_1 + \dot{\beta}_1^2 \cdot \overrightarrow{G_2A} - \ddot{\beta}_1 \cdot \vec{e}_2 \times \overrightarrow{AC} \quad (2)$$

During the second phase, the velocity of point C, belonging to rigid body 2 (pad) is given by:

$$\overrightarrow{v_C} = \vec{u}(G_2) + \dot{\beta}_2 \cdot \vec{e}_2 \times \overrightarrow{G_2C} \quad (3)$$

while the velocity with which the rigid bodies 3 and 4 translate along the linear prismatic guide without friction, along the straight line connecting the position occupied by the two curvature centers at the end of step one, is given by the velocity of point C_3 (Fig. 3b):

$$\overrightarrow{v_{C_3}} = 2 \cdot \vec{u}(G_2) \quad (4)$$

The acceleration of point C, belonging to rigid body 2, is given by (Fig. 3b):

$$\overrightarrow{a_C} = \vec{u}(G_2) + \overrightarrow{a_c}(C) + \ddot{\beta}_2 \cdot \vec{e}_2 \times \overrightarrow{G_2C} = \vec{u}(G_2) + \dot{\beta}_2^2 \cdot \overrightarrow{G_2C} + \ddot{\beta}_2 \cdot \vec{e}_2 \times \overrightarrow{G_2C} \quad (5)$$

and the acceleration of point C_3, is given by:

$$\overrightarrow{a_{C_3}} = 2 \cdot \vec{u}(G_2) \quad (6)$$

2.4 Dynamical Equilibrium

Both mechanical models adopted to study the two phases of the planar motion of the DFP described in previous section are open kinematic chains [17]. And each of them is characterized by one degree of freedom.

In fact, for the first phase, we have 3 rigid bodies, each characterized by 3 kinematic unknowns, for a total of $n = 3 \times 3 = 9$. The number of kinematic constraints is equal to $n_c = 7$ that are given by: a) vertical translation and rotation (2) of the RB1, b) two internal revolute joints ($2 \times 2 = 4$), and c) rotation (1) of the assemblage of RB3 and RB4. The earthquake kinematically controls the translational horizontal degree of freedom of the lowermost sliding plate (RB1). While the rotational degree of freedom of the pad is not known *a priori* so that a force analysis is required and the system equations of motion must be formulated to obtain a number of equations equal to the number of unknown variables.

For the second phase, we have $n = 3 \times 3 = 9$ kinematic unknowns. The number of kinematic constraints is equal to $n_c = 8$ that are given by: a) 3 for the lowermost plate that is assumed fixed, b) 1 for the pad, since its centroid G_2 cannot move orthogonally to the straight line (prismatic frictionless guide) passing through the concave surfaces centers $\overline{C_1C_2}(t_n + \Delta t_1)$, c) 2 for the uppermost sliding plate assembled with the over-structure (RB3+RB4), since they can only translate with the contact point at the end of phase 1 (*i.e.* point C_3 in Fig. 3b) moving along the straight line above, thus neither rotating nor translating orthogonally to that line, and d) 2 are given by the internal constraints constituted by the circular frictional prismatic guides, between the kinematic couples RB1-RB2 and RB2-RB3+RB4, since they do not allow mutual displacement at the contact point, along the relevant radius of curvature. The independent kinematic unknown is $\ddot{\beta}_2$ while the translational acceleration $\ddot{u}(G_2)$ can be expressed as function of $\ddot{\beta}_2$.

The first kinematic chain is both kinematically and dynamically driven [17] since one degree of freedom, that is the horizontal translation of the lowermost plate, is imposed by the ground movement and another, that is the rotation around one of the pad's corners, is governed by the forces involved, either inertia and external. On the other hand, the second kinematic chain is dynamically driven since, for the unknown, a force analysis is required. For both models, a

relevant minimum number of differential equations can be written, in the ambit of the *Embedding Technique* [17], by making a suitable cut in one of the joints among the involved rigid bodies, and formulating the dynamic conditions of the resulting subsystem. The number of these obtained equations, which do not contain the joint reaction forces, is equal to the number of degrees of freedom of the system. Once the minimum number of differential equations are solved, the joint reaction forces can be obtained by the equations of motion obtained by a free-body analysis.

Proceeding in this way, for both phases' kinematic chain, making the cut in correspondence of the revolute joint in point A, the following equilibrium equation, applying the D'Alambert principle, is obtained:

$$\vec{K}_A = \vec{K}_{G_2} + \overrightarrow{AG_2} \times \frac{d}{dt}\vec{Q}_2 + \overrightarrow{AG_3} \times \frac{d}{dt}\vec{Q}_3 + \overrightarrow{AG_4} \times \frac{d}{dt}\vec{Q}_4 = \vec{M}_A = \sum_{i=2}^{4} \overrightarrow{AG_i} \times \vec{P}_i \tag{7}$$

in which: $\vec{K}_A$ is the moment of the inertia forces with respect to point A, $\vec{K}_{G_2}$ is the moment of inertia of RB2 with respect to its centroid, $\vec{Q}_i$ is the momentum of the i-th RB, $\vec{M}_A$ is the moment of the external forces with respect to point A, and $\vec{P}_i$ is the self-weight force of the i-th RB. For each phase, Eq. (7) has to be specialized by substituting, in the expression of the i-th RB time-derivative of the momentum, the kinematically compatible expressions for the accelerations, as obtained in the previous section.

2.5 Thermo-Mechanical Coupling

During the second phase, slipping occurs along the two concave surfaces (Fig. 3b) and heat is developed therein. It is possible both 1) to keep track of the temperature change of the plates and 2) to evaluate the change of the frictional threshold as function of the surface temperature. Thermo-mechanical coupling is obtained by defining a suitable law of variation of the frictional coefficient, as function of the temperature, as follows:

$$F_{\mu i}(t) = \mu_i[T_i(t)] \cdot N_i \tag{8}$$

where: $F_{\mu i}(t)$, μ_i, $T_i(t)$, N_i are a) the friction strength, b) the temperature dependent friction coefficient, c) the temperature, and d) the internal force orthogonal to the i-th concave surface.

At each time step, the increment of Temperature, yielded by the friction-induced heat, can be evaluated by the following thermal equilibrium equation:

$$c_i \cdot \dot{T}_\iota = \dot{Q}_f - \dot{Q}_\iota \tag{9}$$

where: $\dot{T}_\iota$ is the rate of change of temperature ($temperature/time$), c_i is the heat capacity ($energy/temperature$) of the i-th surface, given by the product of the steel specific heat c_s times the mass m_i of the concave surface involved in the heat exchange, $\dot{Q}_f$ and $\dot{Q}_\iota$ are the rate of heat respectively developed and exchanged with the surrounding environment ($energy/time$). For the sake of simplicity, m_i may be assumed coincident with the whole mass of the relevant steel plate (Fig. 1).

Moreover, the following assumptions may be made: 1) heat is generated by friction at each of the sliding interfaces, 2) heat conduction is assumed unidirectional, perpendicular to each concave surface, 3) heat loss due to radiation is assumed negligible, 4) bearing material (PTFE or the like) is assumed as a perfect thermal insulator so that heat generated at the sliding interface just flows towards each concave surface (in fact the thermal diffusivity of steel is

$\sim 20.0\, W/m \cdot °C$ that is much larger than the one of PTFE $\sim 0.24\, W/m \cdot °C$ at $20°C$ temperature).

The rate of heat exchange $\dot{Q}_i(\mathrm{T}, \mathrm{t})$ by the i-th surface with the surrounding environment can be modelled by the Newton's law of cooling that is usually adopted to describe convective heat exchanges, that is:

$$\dot{Q}_i(T,t) = H_i \cdot (T_i - T_{air}) \tag{10}$$

where: H_i is the i-th concave surface heat transfer coefficient ($heat/temperature \cdot time$), given by the product of the steel convectional heat exchange coefficient h_s times the area A_i of the portion of the concave surface effectively exchanging heat with the surrounding air whose temperature is T_{air}.

3 SOLVING EQUATIONS

Given the modelling strategy singled out in the previous sections, the relevant equations are herein developed. Note that given the complexity of the topic, the solving equations herein presented, along with both formal exposition and numerical solution strategy, may be revised and optimized in further future developments, according to more advanced solution strategies developed for the multi-body dynamics (*e.g.* [18,19]]. However, it must be stressed that further complexity is brought by the fact that the several internal constraints, differently from what happens in the case of conventional multi-body mechanical devices, change either position in the reference system (the revolute joints along the concave surfaces) or the orientation (the prismatic frictionless guides) during the deformation time-history.

3.1 First phase

Referring to other documents for further details [15-16], previous Eq. (7) can be written as follows:

$$\begin{aligned} -J_{2y} \cdot \ddot{\beta}_1 + m_2 \cdot \left(a_{G_2}\right)_x \cdot \left(\overline{AG_2}\right)_z + m_3 \cdot \left(a_{G_3}\right)_x \cdot \left(\overline{AG_3}\right)_z + m_4 \cdot \left(a_{G_4}\right)_x \cdot \left(\overline{AG_4}\right)_z \\ - m_2 \cdot \left(\overline{AG_2}\right)_x \cdot \left[g + \left(a_{G_2}\right)_z\right] - m_3 \cdot \left(\overline{AG_3}\right)_x \cdot \left[g + \left(a_{G_3}\right)_z\right] - m_4 \\ \cdot \left(\overline{AG_4}\right)_x \cdot \left[g + \left(a_{G_4}\right)_z\right] = 0 \end{aligned} \tag{11}$$

where: J_{2y} is the pad's centroid mass moment of inertia around axis y, m_i is the mass of the i-th rigid body involved, g is the acceleration of gravity, $\left(\overline{AG_i}\right)_x$ and $\left(\overline{AG_i}\right)_z$ are the components, along the reference system's axes, of the vectors connecting point A to the i-th rigid body centroid, $\left(a_{G_i}\right)_x$ and $\left(a_{G_i}\right)_z$ are the components of the i-th rigid body centroid's acceleration (Fig. 4).

Since in the numerical solution the incremental time step will be assumed suitably small, angle β_1 can be assumed very small so that the following expressions hold:

$$\beta_1 \cong 0 \rightarrow \begin{cases} \sin\beta_1 \cong \beta_1 \\ \cos\beta_1 \cong 1 \end{cases} \tag{12}$$

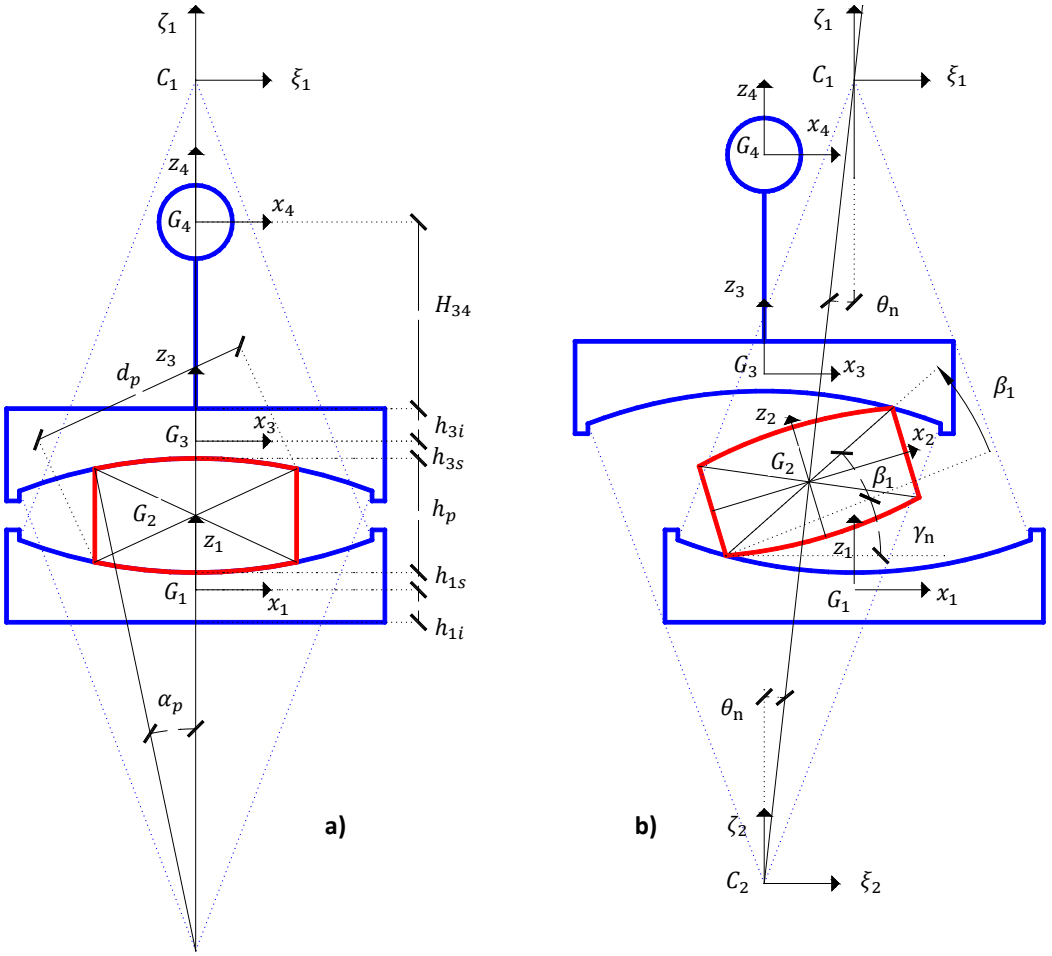

Figure 4. First phase: a) several geometrical quantities and b) deformed configuration for β_1 (rotation).

By introducing the explicit expressions of the several terms, and taking into consideration the simplification of Eq. (12), Eq. (11) can be rewritten as follows:

$$a_{11} \cdot \ddot{\beta}_1 + a_{12} \cdot \dot{\beta}_1^2 + a_{13} \cdot \beta_1 + a_{14} + a_{15} \cdot \ddot{\beta}_1 \cdot \beta_1 + a_{16} \cdot \dot{\beta}_1^2 \cdot \beta_1 + a_{17} \cdot \ddot{\beta}_1 \cdot \beta_1^2 + a_{18} \cdot \dot{\beta}_1^2 \cdot \beta_1^2 = 0 \quad (13)$$

where the coefficients are given by:

$$a_{11} = -J_{2y} - \left(\frac{m_2 \cdot h_{21}}{2} + m_3 \cdot h_{31} + m_4 \cdot h_{41}\right) \cdot d_p \cdot \sin\gamma_n - \left(\frac{m_2 \cdot k_{21}}{2} + m_3 \cdot k_{31} + m_4 \cdot k_{41}\right) \cdot d_p \cdot \cos\gamma_n \quad (14)$$

$$a_{12} = -\left(\frac{m_2 \cdot h_{21}}{2} + m_3 \cdot h_{31} + m_4 \cdot h_{41}\right) \cdot d_p \cdot \cos\gamma_n + \left(\frac{m_2 \cdot k_{21}}{2} + m_3 \cdot k_{31} + m_4 \cdot k_{41}\right) \cdot d_p \cdot \sin\gamma_n \quad (15)$$

$$a_{13} = \left(\frac{m_2}{2} + m_3 + m_4\right) \cdot d_p \cdot \ddot{x}_g \cdot \cos\gamma_n + \left(\frac{m_2}{2} + m_3 + m_4\right) \cdot d_p \cdot g \cdot \sin\gamma_n \quad (16)$$

$$a_{14} = (m_2 \cdot h_{21} + m_3 \cdot h_{31} + m_4 \cdot h_{41}) \cdot \ddot{x}_g - (m_2 \cdot k_{21} + m_3 \cdot k_{31} + m_4 \cdot k_{41}) \cdot g \quad (17)$$

$$a_{15} = -\left(\frac{m_2 \cdot h_{21}}{2} + m_3 \cdot h_{31} + m_4 \cdot h_{41}\right) \cdot d_p \cdot \cos\gamma_n + \left(\frac{m_2 \cdot k_{21}}{2} + m_3 \cdot k_{31} + m_4 \cdot k_{41}\right) \cdot d_p \cdot \sin\gamma_n - \left(\frac{m_2}{4} + m_3 + m_4 - \frac{m_2}{4} - m_3 - m_4\right) \cdot d_p^2 \cdot \cos\gamma_n \cdot \sin\gamma_n \tag{18}$$

$$a_{16} = \left(\frac{m_2 \cdot h_{21}}{2} + m_3 \cdot h_{31} + m_4 \cdot h_{41}\right) \cdot d_p \cdot \sin\gamma_n + \left(\frac{m_2 \cdot k_{21}}{2} + m_3 \cdot k_{31} + m_4 \cdot k_{41}\right) \cdot d_p \cdot \cos\gamma_n - \left(\frac{m_2}{4} + m_3 + m_4\right) \cdot d_p^2 \cdot \cos^2\gamma_n + \left(-\frac{m_2}{4} - m_3 - m_4\right) \cdot d_p^2 \cdot \sin^2\gamma_n \tag{19}$$

$$a_{17} = -\left(\frac{m_2}{4} + m_3 + m_4\right) \cdot d_p^2 \cdot \cos^2\gamma_n - \left(\frac{m_2}{4} + m_3 + m_4\right) \cdot d_p^2 \cdot \sin^2\gamma_n = -\left(\frac{m_2}{4} + m_3 + m_4\right) \cdot d_p^2 \tag{20}$$

$$a_{18} = \left(\frac{m_2}{4} + m_3 + m_4 - \frac{m_2}{4} - m_3 - m_4\right) \cdot d_p^2 \cdot \sin\gamma_n \cdot \cos\gamma_n = 0 \tag{21}$$

$$h_{21} = \frac{d_p}{2} \cdot \sin\gamma_n \tag{22}$$

$$h_{31} = h_{3s} + h_p \cdot \cos\theta_n + 2 \cdot R_1 \cdot (1 - \cos\theta_n) - R_1 \cdot \left[1 - \cos\left(\theta_n + \alpha_p\right)\right] \tag{23}$$

$$h_{41} = h_{31} + H_{34} = h_{3s} + H_{34} + h_p \cdot \cos\theta_n + 2 \cdot R_1 \cdot (1 - \cos\theta_n) - R_1 \cdot \left[1 - \cos\left(\theta_n + \alpha_p\right)\right] \tag{24}$$

$$k_{21} = \frac{d_p}{2} \cdot \cos\gamma_n \tag{25}$$

$$k_{31} = R_1 \cdot \sin\left(\theta_n + \alpha_p\right) - 2 \cdot \left(R_1 - \frac{h_p}{2}\right) \cdot \sin\theta_n \tag{26}$$

$$k_{41} = R_1 \cdot \sin\left(\theta_n + \alpha_p\right) - 2 \cdot \left(R_1 - \frac{h_p}{2}\right) \cdot \sin\theta_n = k_{31} \tag{27}$$

and the meaning of the geometrical quantities can be found in Fig. 4.

Oversimplifying the above assumption of infinitesimal value of the angle β_1, we may assume that:

$$\beta_1 \to 0 \to \begin{cases} \sin\beta_1 \cong 0 \\ \cos\beta_1 \cong 1 \end{cases} \tag{28}$$

and Eq. (13) may be rewritten, also neglecting the higher order infinitesimals, as follows:

$$a_{11} \cdot \ddot{\beta}_1 + a_{12} \cdot \dot{\beta}_1^2 + a_{14} = 0 \tag{29}$$

3.2 Geometric compatibility at the end of the first phase

The value of the rotation β_1^* undergone by the pad around point *A* can be obtained by solving the governing equation of the first phase, *i.e.* either Eq. (13) or Eq. (29).

The value of the angle θ_{n+1} that the line $\overline{C_1C_2}$ connecting the two concave surfaces centers forms with the ζ_1 axis at the end of the first time step can be obtained, by means of geometric relationships, as follows:

$$\theta_{n+1} = \frac{\pi}{2} - \tan^{-1}\widetilde{m} = \frac{\pi}{2} - \tan^{-1}\frac{\zeta_1[G_2(t_n + \Delta t_1^*)]}{\xi_1[G_2(t_n + \Delta t_1^*)]} \tag{30}$$

where:

$$\xi_1\left[G_2\left(t_n + \Delta t_1\right)\right] = \xi_{1A} - \sqrt{\xi_{1A}^2 - C} \tag{31}$$

$$\zeta_1\left[G_2\left(t_n+\Delta t_1\right)\right]=\zeta_{1A}-\left[\tan\left(\gamma_n+\beta_1^*\right)\right]\cdot\sqrt{\xi_{1A}^2-C} \tag{32}$$

$$C=\frac{\xi_{1A}^2\cdot\tan^2\left(\gamma_n+\beta_1^*\right)-d_p^2/4}{1+\tan^2\left(\gamma_n+\beta_1^*\right)} \tag{33}$$

in which: Eq. (31) and Eq. (32) are the coordinates of the pad centroid G_2 in the reference system $C_1\xi_1\zeta_1$ at the end of the previous phase of the current time step Δt_1 ; $\xi_{1A}=\xi_1[A(t_n)]$ and $\zeta_{1A}=\zeta_1[A(t_n)]$ are the coordinates of the pad vertex A in the reference system $C_1\xi_1\zeta_1$ at the end of the previous time step t_n. The coordinates ξ_{1A} and ζ_{1A} will be evaluated as further specified in the following text.

The angle β_2^* of which the pad has to counter-rotate, during the second phase (Fig. 5), around its centroid to restore geometric compatibility, which means in order for the pad axis to superimpose to the straight line passing through the two concave surfaces' centers, can be obtained, by mere goniometric relationships, as follows:

$$\beta_2^*=\gamma_n+\beta_1^*+\psi_1-\left(\frac{\pi}{2}-\theta_{n+1}\right) \tag{34}$$

where ψ_1 is an angle characteristic of the pad own geometry (Fig. 1).

3.3 Second phase

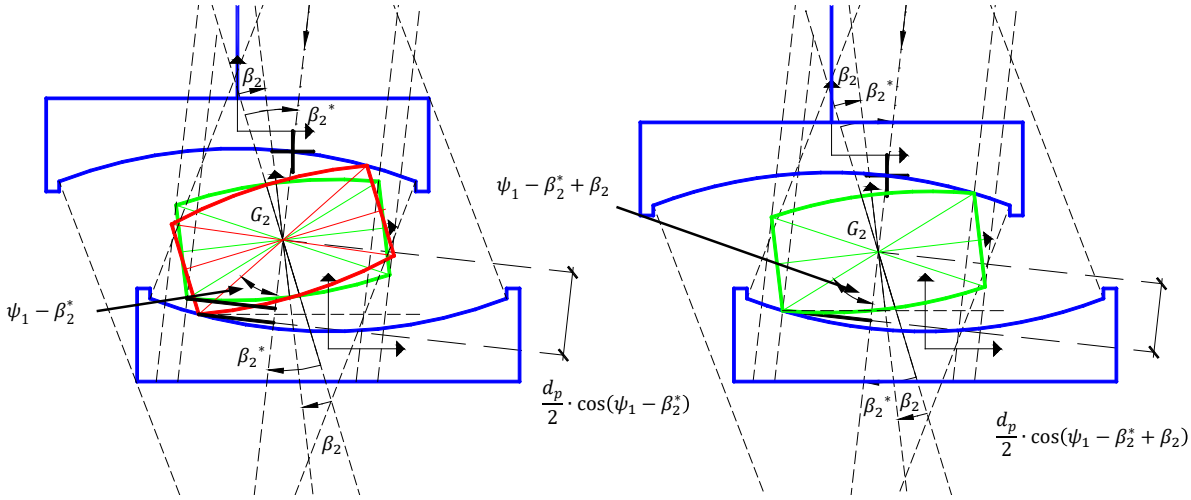

Figure 5. Second phase: relationship between dependent kinematic variable $u(G_2)$ (displacement) and independent kinematic variable β_2 (rotation).

As already explained, during the second phase (Fig. 5), the pad counter-rotates and translates with its centroid moving along the straight line connecting the two concave surfaces' centers $\overline{C_1C_2}$. Since the independent variable is one only, the relationship between the centroid translation $u(G_2)$ and the counter-rotation β_2 can be expressed as follows:

$$u(G_2)=\frac{d_p}{2}\cdot\left[(1-\cos\beta_2)\cdot\cos(\psi_1-\beta_2^*)+\sin\beta_2\cdot\sin(\psi_1-\beta_2^*)\right] \tag{35}$$

Such approximation consists in neglecting the presence of the curvature of the concave surface in determining the relationship between translation and rotation. Such approximation is based on a twofold reason, that is: 1) the amplitude of the concave surfaces radius R_1 is very

large, and to 2) the fact that the solution of the model will be implemented by means of a numerical strategy, thus discretizing the angle increment by very small amounts.

The velocity of translation of centroid G_2 is given by:

$$\dot{u}(G_2) = \frac{d_p}{2} \cdot \dot{\beta}_2 \cdot \sin\beta_2 \cdot \cos(\psi_1 - \beta_2^*) + \frac{d_p}{2} \cdot \dot{\beta}_2 \cdot \cos\beta_2 \cdot \sin(\psi_1 - \beta_2^*) \tag{36}$$

and the acceleration by:

$$\begin{aligned} \ddot{u}(G_2) = \frac{d_p}{2} \cdot \left(\dot{\beta}_2^2 \cdot \cos\beta_2 + \ddot{\beta}_2 \cdot \sin\beta_2\right) \cdot \cos(\psi_1 - \beta_2^*) + \frac{d_p}{2} \\ \cdot \left(-\dot{\beta}_2^2 \cdot \sin\beta_2 + \ddot{\beta}_2 \cdot \cos\beta_2\right) \cdot \sin(\psi_1 - \beta_2^*) \end{aligned} \tag{37}$$

Concluding, Eq. (7) for the second phase becomes:

$$\begin{aligned} J_{2y} \cdot \ddot{\beta}_2 + \left[m_2 \cdot \left(\overline{AG_2}\right)_x + 2 \cdot m_3 \cdot \left(\overline{AG_3}\right)_x + 2 \cdot m_4 \cdot \left(\overline{AG_4}\right)_x\right] \cdot \ddot{u}(G_2) \cdot \cos\theta_{n+1} \\ - \left[m_2 \cdot \left(\overline{AG_2}\right)_z + 2 \cdot m_3 \cdot \left(\overline{AG_3}\right)_z + 2 \cdot m_4 \cdot \left(\overline{AG_4}\right)_z\right] \cdot \ddot{u}(G_2) \cdot \sin\theta_{n+1} \\ - \left[m_2 \cdot g \cdot \left(\overline{AG_2}\right)_x + m_3 \cdot g \cdot \left(\overline{AG_3}\right)_x + m_4 \cdot g \cdot \left(\overline{AG_4}\right)_x\right] = 0 \end{aligned} \tag{38}$$

that, with the simplification of Eq. (12), becomes:

$$\begin{aligned} a_{21} \cdot \ddot{\beta}_2 + a_{22} \cdot \dot{\beta}_2^2 + a_{23} \cdot \beta_2 + a_{24} + a_{25} \cdot \ddot{\beta}_2 \cdot \beta_2 + a_{26} \cdot \dot{\beta}_2^2 \cdot \beta_2 + a_{27} \cdot \ddot{\beta}_2 \cdot \beta_2^2 \\ + a_{28} \cdot \dot{\beta}_2^2 \cdot \beta_2^2 = 0 \end{aligned} \tag{39}$$

where the coefficients are given by:

$$a_{21} = J_{2y} + \frac{d_p}{2} \cdot (l_{21} \cdot \cos\theta_{n+1} - l_{22} \cdot \sin\theta_{n+1}) \cdot \sin(\psi_1 - \beta_2^*) \tag{40}$$

$$a_{22} = \frac{d_p}{2} \cdot (l_{21} \cdot \cos\theta_{n+1} - l_{22} \cdot \sin\theta_{n+1}) \cdot \cos(\psi_1 - \beta_2^*) \tag{41}$$

$$a_{23} = -n_{23} \tag{42}$$

$$a_{24} = -l_{23} \tag{43}$$

$$\begin{aligned} a_{25} = n_{21} \cdot \frac{d_p}{2} \cdot \sin(\psi_1 - \beta_2^*) \cdot \cos\theta_{n+1} + l_{21} \cdot \frac{d_p}{2} \cdot \cos(\psi_1 - \beta_2^*) \cdot \cos\theta_{n+1} - n_{22} \cdot \frac{d_p}{2} \\ \cdot \sin(\psi_1 - \beta_2^*) \cdot \sin\theta_{n+1} - l_{22} \cdot \frac{d_p}{2} \cdot \cos(\psi_1 - \beta_2^*) \cdot \sin\theta_{n+1} \end{aligned} \tag{44}$$

$$\begin{aligned} a_{26} = n_{21} \cdot \frac{d_p}{2} \cdot \cos(\psi_1 - \beta_2^*) \cdot \cos\theta_{n+1} - l_{21} \cdot \frac{d_p}{2} \cdot \sin(\psi_1 - \beta_2^*) \cdot \cos\theta_{n+1} - n_{22} \cdot \frac{d_p}{2} \\ \cdot \cos(\psi_1 - \beta_2^*) \cdot \sin\theta_{n+1} + l_{22} \cdot \frac{d_p}{2} \cdot \sin(\psi_1 - \beta_2^*) \cdot \sin\theta_{n+1} \end{aligned} \tag{45}$$

$$a_{27} = \frac{d_p}{2} \cdot (n_{21} \cdot \cos\theta_{n+1} - n_{22} \cdot \sin\theta_{n+1}) \cdot \cos(\psi_1 - \beta_2^*) \tag{46}$$

$$a_{28} = -\frac{d_p}{2} \cdot (n_{21} \cdot \cos\theta_{n+1} + n_{22} \cdot \sin\theta_{n+1}) \cdot \sin(\psi_1 - \beta_2^*) \tag{47}$$

$$l_{21} = d_p \cdot \cos(\gamma_n + \beta_1^*) \cdot \left(\frac{m_2}{2} + 2 \cdot m_3 + 2 \cdot m_4\right) - 2 \cdot (m_3 + m_4) \cdot R_1 \cdot \sin\left(\theta_{n+1} + \alpha_p\right) \tag{48}$$

$$n_{21} = d_p \cdot \sin(\gamma_n + \beta_1^*) \cdot \left(\frac{m_2}{2} + 2 \cdot m_3 + 2 \cdot m_4\right) \tag{49}$$

$$l_{22} = d_p \cdot \sin(\gamma_n + \beta_1^*) \cdot \left(\frac{m_2}{2} + 2 \cdot m_3 + 2 \cdot m_4\right) - 2 \cdot (m_3 + m_4) \cdot R_1 \cdot \cos\left(\theta_{n+1} + \alpha_p\right) + 2 \cdot (m_3 + m_4 +) \cdot h_{3s} + 2 \cdot m_4 \cdot H_{34} \tag{50}$$

$$n_{22} = -d_p \cdot \cos(\gamma_n + \beta_1^*) \cdot \left(\frac{m_2}{2} + 2 \cdot m_3 + 2 \cdot m_4\right) \tag{51}$$

$$l_{23} = d_p \cdot g \cdot \cos(\gamma_n + \beta_1^*) \cdot \left(\frac{m_2}{2} + m_3 + m_4\right) - (m_3 + m_4) \cdot g \cdot R_1 \cdot \sin\left(\theta_{n+1} + \alpha_p\right) \tag{52}$$

$$n_{23} = d_p \cdot g \cdot \sin(\gamma_n + \beta_1^*) \cdot \left(\frac{m_2}{2} + m_3 + m_4\right) \tag{53}$$

Oversimplifying as indicated in Eq. (25) and neglecting the higher order infinitesimals, Eq. (36) may be rewritten as follows:

$$a_{21} \cdot \ddot{\beta}_2 + a_{22} \cdot \dot{\beta}_2^2 + a_{24} = 0 \tag{54}$$

3.4 Geometric compatibility at the end of the second phase

Once the angle θ_{n+1} has been determined, also the new value γ_{n+1} of the inclination of the diagonal $\overline{AC}$ with respect to the horizontal overall axis x can be determined, with simple goniometric relationships (Fig. 4 above), as follows:

$$\gamma_{n+1} = \pi - \psi_1 - \left(\frac{\pi}{2} + \theta_{n+1}\right) = \frac{\pi}{2} - \psi_1 - \theta_{n+1} \tag{55}$$

where θ_{n+1} is herein assumed positive if it is oriented clockwise.

3.5 Free body analysis

For each one of the two phases, after having solved the relevant governing differential equation, the constraint forces can be determined by means of the dynamic conditions written for each single rigid body.

The unit vectors, either tangent $\vec{\tau}_{ij}$ or orthogonal $\vec{n}_{ij}$ to the concave surfaces in correspondence of the contact point between the i-th and j-th rigid bodies, are as follows (Fig. 6):

$$\vec{\tau}_{21}(A) = \cos(\theta + \alpha) \cdot \vec{e}_1 - \sin(\theta + \alpha) \cdot \vec{e}_3 \tag{56}$$

$$\vec{n}_{21}(A) = \sin(\theta + \alpha) \cdot \vec{e}_1 + \cos(\theta + \alpha) \cdot \vec{e}_3 \tag{57}$$

$$\vec{\tau}_{23}(C) = -\cos(\theta + \alpha) \cdot \vec{e}_1 + \sin(\theta + \alpha) \cdot \vec{e}_3 \tag{58}$$

$$\vec{n}_{23}(C) = -\sin(\theta + \alpha) \cdot \vec{e}_1 - \cos(\theta + \alpha) \cdot \vec{e}_3 \tag{59}$$

where the value of the angles θ and α depends on the phase, either first or second (Fig. 6).

The dynamic conditions for the free-body diagrams are as follows:

$$m_1 \cdot \left(a_{G_1}\right)_x \cdot \vec{e}_1 = \left[N_{12} \cdot \vec{n}_{12}(A) + T_{12} \cdot \vec{\tau}_{12}(A) + N_{23} \cdot \vec{n}_{23}(C) + \ddot{x}_g\right] \cdot \vec{e}_1 \tag{60}$$

$$m_2 \cdot \left(a_{G_2}\right)_x \cdot \vec{e}_1 = [N_{21} \cdot \vec{n}_{21}(A) + T_{21} \cdot \vec{\tau}_{21}(A) + N_{23} \cdot \vec{n}_{23}(C) + T_{23} \cdot \vec{\tau}_{23}(C)] \cdot \vec{e}_1 \tag{61}$$

$$m_2 \cdot \left(a_{G_2}\right)_z \cdot \vec{e}_3 = [N_{21} \cdot \vec{n}_{21}(A) + T_{21} \cdot \vec{\tau}_{21}(A) + N_{23} \cdot \vec{n}_{23}(C) + T_{23} \cdot \vec{\tau}_{23}(C) - m_2 \cdot g] \cdot \vec{e}_3 \tag{62}$$

$$m_2 \cdot J_{2y} \cdot \vec{e}_2 = [N_{21} \cdot \vec{n}_{21}(A) + N_{23} \cdot \vec{n}_{23}(C)] \cdot \frac{d_p}{2} \cdot \cos\gamma \cdot \vec{e}_3 + [T_{21} \cdot \vec{\tau}_{21}(A) + T_{23} \cdot \vec{\tau}_{23}(C)] \cdot \frac{d_p}{2} \cdot \sin\gamma \cdot \vec{e}_1 \tag{63}$$

$$(m_3 + m_4) \cdot \left(a_{G_{34}}\right)_x \cdot \vec{e}_1 = [N_{32} \cdot \vec{n}_{32}(C) + T_{32} \cdot \vec{\tau}_{32}(C)] \cdot \vec{e}_1 \tag{64}$$

$$(m_3 + m_4) \cdot \left(a_{G_{34}}\right)_z \cdot \vec{e}_3 = [N_{32} \cdot \vec{n}_{32}(C) + T_{32} \cdot \vec{\tau}_{32}(C) - (m_3 + m_4) \cdot g] \cdot \vec{e}_3 \tag{65}$$

where: the value assumed by the angle γ depends on the phase (Fig. 6). For the given interface between rigid bodies i and j, the constraint force can be split in the two components: 1) the one N_{ij} orthogonal to the concave surface, and 2) the one $T_{ij} = \mu \cdot N_{ij}$ tangent to it (Fig. 6), where μ is the Coulomb's friction coefficient. In particular, given the assumption of Coulomb friction at each $i - j$ interface, and the relevant relationship between the two components of the constraint force, for each phase, two equations only are needed to determine these latter.

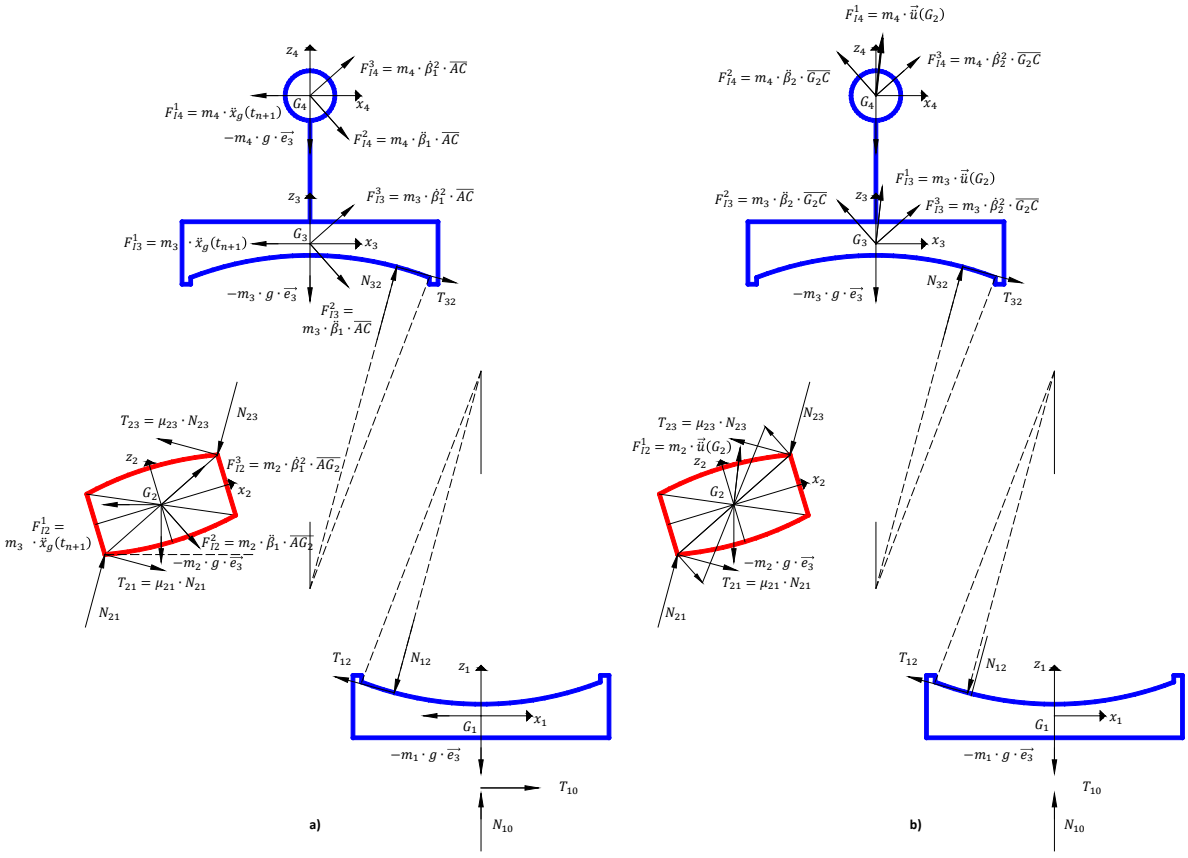

Figure 5. Free body-diagrams of the open kinematic chain corresponding to a) the first phase, of sticking, and b) the second phase, of slipping.

3.6 Heat developed

The heat developed during the second phase of the current time step, which means during the contextual pointwise (Fig. 3) frictional sliding, can be evaluated as follows:

$$Q_f(t_{n+1}) = \int_{\theta_n}^{\theta_{n+1}} T_{21} \cdot R \cdot d\theta + \int_{\theta_n}^{\theta_{n+1}} T_{23} \cdot R \cdot d\theta \tag{66}$$

Such heat is necessary to update, stepwise, the friction coefficient and relevant sliding threshold, according to Eq. (8).

4 CONCLUSIONS

The currently accepted theory about the mechanical behavior of the friction pendulum devices presents some drawbacks. In fact: a) these devices are studied only considering planar deformation, b) equilibrium is considered only along the horizontal direction, completely neglecting both the vertical and rotational ones, and c) it is assumed that sliding occurs along a very strict sequence of coupled surfaces. Moreover, from a strict mechanical standpoint: a) it is not clear how the geometrical compatibility is respected during the deformations induced by a seismic attack, b) contact mechanics-related theories warn about the possibility that such devices undergo the so-called stick-slip phenomenon. From a tribological standpoint, it is not clear which is the most suitable frictional coefficient and the relevant liner to assure it.

The wish to contribute to a better understanding of the mechanical behavior of such complex tribological systems has brought the authors to develop a new modelling strategy. Such model basically originates from a new assumption about the way in which the geometrical compatibility is fulfilled during the relative movement that the rigid components undergo during the kinematic time-history imposed by the shaking ground. Beyond the pure mechanical behavior, attention was also focused on the thermo-mechanical aspects, in order to figure out the order of magnitude of friction-induced temperatures and their effect on the friction coefficient. Ultimately, the interest is to find the most suitable liner in order to prevent a temperature-induced increase of the friction coefficient with consequent re-coupling of ground shaking and structure movement.

The proposed modelling strategy assumes that at each time increment of the discretized time-history, the FPS undergoes a two-step deformation in order to re-establish the geometric compatibility. An assemblage of rigid bodies, differently constrained between each other, models each of these phases. The first phase envisages that, due to the horizontal translation of the lower plate, the internal pad, pinpointed at the two sliding plates, rigidly rotates around the lower extremity of one of the two diagonals while the superstructure, composed by the rigid assemblage of both upper plate and overlying structure, rigidly translates along horizontal and vertical directions. The second phase envisages that, with the lower plate still, the internal pad is constrained to the two concave-surfaced sliding plates by frictional cylindrical guides while the superstructure is constrained to translate only with a point moving along a frictionless linear guide. The pad rigidly roto-translates with its centroid moving along the straight line connecting the two spherical surfaces' centers while the superstructure rigidly translates along the same line. Frictional slippage occurs point-wise along the extremities of one of the two diagonals of the pad, yielding heat production. The two phases also clearly define the stick-slip phenomenon. Due to the evolutionary process of the constraints between each other of the rigid sub-components, the ensuing mechanical behavior is highly nonlinear.

Only one kinematic unknown characterizes each of the two phases. The so-called Embedding technique was herein implemented. According to this latter, only one differential equation can be written for each phase, by making a suitable cut in one of the joints among the rigid sub-components, and formulating the dynamic equilibrium of the resulting sub-system. After solv-

ing the governing differential equation, the joint reaction forces can be obtained by the equations of motions obtained by a free-body analysis. The details of the numerical strategy were presented even though it is still undergoing a fine-tuning and optimization review process.

The numerical strategy will be implemented in a calculation spreadsheet and parametric studies will be carried out. The numerical results will be compared with available experimental results in order to hopefully confirm the assumptions herein made. Further research is needed.

From a physical standpoint, the following improvements may be brought. First, the assumption of restoration of the kinematic compatibility at each time step, with consequent closure of the kinematic pairs, may be removed thus accounting for the likely dependence of the stick-slip phenomenon on the frequency content of the seismic waves. Secondly, the likelihood of impact between the pad and the concave surfaces at restoration of the geometric compatibility may be also taken into account. In fact, the impact-induced force may break the components involved. Moreover, the mechanical behavior may be studied three-dimensionally.

REFERENCES

[1] V.A. Zayas, S.S. Low, S.A. Mahin, The FPS earthquake resisting system, Report No. 87-01, Earthquake Engineering Research Center, Berkley, CA, 1987.

[2] A. Mokha, M. Constantinou, A. Reinhorn, Teflon bearings in base isolation, I: testing. *ASCE Journal of Structural Engineering*, **116(2)**, 438-454, 1990.

[3] M. Constantinou, A. Mokha, A. Reinhorn, Teflon bearings in base isolation, II: modeling. *ASCE Journal of Structural Engineering*, **116(2)**, 455-474, 1990.

[4] D.M. Fenz, M.C. Constantinou, Behaviour of the double concave Friction Pendulum bearing. *Earthquake Engineering and Structural Dynamics*, **35**, 1403-1424, 2006.

[5] D.M. Fenz, M.C. Constantinou, Spherical sliding isolation bearings with adaptive behavior: Experimental verification. *Earthquake Engineering and Structural Dynamics*, **37**, 185-205, 2008.

[6] T.C. Becker, S.A. Mahin, Experimental and analytical study of the bi-directional behavior of the triple friction pendulum isolator. *Earthquake Engineering and Structural Dynamics*, **41(3)**, 355-373, 2012.

[7] T.C. Becker, S.A. Mahin, Correct treatment of rotation of sliding surfaces in a kinematic model of the triple friction pendulum bearing. *Earthquake Engineering and Structural Dynamics*, **42(2)**, 311-317, 2012.

[8] C.S. Tsai, Y.C. Lin, H.C. Su, Characterization and modeling of multiple friction pendulum system with numerous sliding interfaces. *Earthquake Engineering and Structural Dynamics*, **39(13)**, 1463-1491, 2010.

[9] S. Nagarajaiah, A.M. Reinhorn, M.C. Constantinou, Nonlinear dynamic analysis of 3D base isolated structures. *ASCE Journal of Structural Engineering*, **117(7)**, 2035-2054, 1991.

[10] V. Popov, *Contact Mechanics and friction – physical principles and applications*. Springer, Berlin, 2010.

[11] G. Scotto Lavina, *Riassunto delle Lezioni di Meccanica Applicata alle Macchine*. Edizioni Scientifiche Siderea, 1990.

[12] N.P. Belfiore, A. Di Benedetto, E. Pennestrì, *Fondamenti di meccanica applicata alle macchine*. Casa Editrice Ambrosiana, 2000.

[13] Italian Technical Regulations, Norme Tecniche per le Costruzioni, NTC2008, Italy.

[14] UNI EN 1998-1, Eurocode 8 - Design of structures for earthquake resistance - Part 1: General rules, seismic actions and rules for buildings. CEN European Committee for Standardization.

[15] V. Bianco, G. Monti, N.P. Belfiore, New approach to model the mechanical behavior of the multiple friction pendulum devices. *5th International conference on Integrity, Reliability and Failure (IRF2016)*, Porto, Portugal, July 24-28, 2016.

[16] V. Bianco, G. Monti, N.P. Belfiore, Mechanical Modelling of Friction Pendulum Isolation Devices. New approach to model the mechanical behavior of the multiple friction pendulum devices. *Italian Concrete Days, Giornate AICAP 2016 – Congresso CTE, (ICD2016),* Rome, Italy, October 27-28, 2016.

[17] A.A. Shabana, *Computational Dynamics*. John Wiley & Sons, New York, 2001.

[18] L. Mariti, N.P. Belfiore, E. Pennestrì, P.P. Valentini, Comparison of solution strategies for multibody dynamics equations. *International Journal for Numerical Methods in Engineering*, **88(7)**, 637-656, 2011.

[19] A.A. Shabana, *Dynamics of Multibody Systems*. John Wiley & Sons, New York, 1989.